

March 17, 2021

Ac-induced thermal vortex escape in magnetic-field-embedded long annular Josephson junctions

Niels Grønbech-Jensen

Department of Applied Science, University of California, Davis, California 95616.

Matteo Cirillo

Department of Physics and INFM, University of Rome "Tor Vergata", I-00133 Rome, Italy.

Abstract

We investigate theoretically the thermal escape behavior of trapped magnetic fluxons in long annular Josephson junctions in dc magnetic fields, and perturbed by a probing ac current. The study is motivated by recently published experimental data that show multi-peaked escape distributions for increasing bias current in the extreme low temperature regime when the system is perturbed by an ac current. We demonstrate that the observed behavior of multi-peaked escape distributions can be reproduced and predicted in the entirely classical, thermally driven sine-Gordon model, which is widely accepted as accurately describing the experimental system. We interpret the observed multi-peaked distributions as being directly induced by dynamical resonances between the applied ac perturbation and the natural oscillation frequency of a trapped fluxon.

PACS numbers: 85.25.-j, 85.25.Cp, 74.50.+r

Several experiments have suggested^{1,2} that Josephson junctions, operated in their zero-voltage state and close to the critical current, will reveal signatures of quantum levels if perturbed by ac currents at frequencies which, when multiplied with Planck's constant, correspond to the energy between the anticipated levels. The signatures are found by slowly increasing the dc bias current of the junction and recording the current at which the voltage across the junction switches from zero to a non-zero value. By repeating such experiments, one can obtain a distribution of critical switching currents, which reflects aspects of the nature of the switching device. These studies have been inspired by extensively conducted work over the past three decades confirming the consistency between Kramers theory for *thermal* escape with the predicted behavior of superconducting devices at non-zero temperature for various kinds of Josephson junction systems^{3,4,5,6,7,8}. Given the consistency in the classical, thermal regime of Josephson junctions, similar escape measurements in the low temperature regime, where quantum uncertainty should dominate thermal fluctuations, have been conducted. These have provided the possibility for non-thermal features in the measurable switching distribution. A specific aim has been to identify signatures of quantum levels expected in the extreme low temperature regime of the zero-voltage junction. Such energy levels could manifest themselves through the escape statistics if more than one energy level is statistically possible, since a junction in an excited energy state will have a higher probability of switching at lower bias currents than a junction in the ground state. Thus, if multiple quantum levels can be populated, then the switching current distribution may reflect this as a multi-peaked profile, each peak identifying a unique quantum level. Experimental efforts have identified and reported such multi-peaked switching distributions in a variety of Josephson junction systems with application of a small ac current. The rationale for this ac perturbation is that it provides the energy (at a particular frequency) to populate specific excited energy levels.

A particularly noticeable set of observations was reported for an annular long Josephson junction in a static magnetic field, and with a single trapped magnetic flux quantum⁹. This system is known^{10,11} to exhibit behavior similar to that of a small-area Josephson junction, and thus, should behave equivalently to small area junctions when conducting switching measurements⁶. Since a magnetic fluxon is a macroscopic object, anomalous switching behavior related to the fluxon dynamics would imply that macroscopic quantum dynamics had been identified. It is the aim of this paper to investigate what can be expected from an

equivalent purely classical model of the system, and compare the results to the published experimental results to assess the interpretation of the experiments. Thus, the physical object of our investigations is an annular Josephson junction of inner radius R and width W in the limit that the length of the junction $2\pi(R + W/2)$ is much larger than the Josephson penetration depth¹². The total area of the junction is $(\pi W^2 + 2\pi RW)$ and therefore, if the width is much less than the inner radius, a good approximation for the area of the annular junction is $2\pi RW$. We make this last assumption, but we also assume that the width of the junction is smaller than the Josephson penetration depth, meaning that we restrict our interest to one-dimensional physics along the barrier forming the junction. In this limit, relevant electrical parameters are the capacitance (\mathcal{C}), inductance (\mathcal{L}), and the sub-gap conductance (\mathcal{G}) per unit length of the junction. For the case of the annular junction that we consider, $\mathcal{C} = \varepsilon_0 \varepsilon_r W / \mathcal{T}$ and $\mathcal{L} = \mu_0 D / W$. Here, ε_0 and μ_0 are, respectively, the vacuum permittivity and permeability and ε_r is the relative dielectric constant of the oxide of the junction. The parameter \mathcal{T} represents the thickness of the oxide barrier while the parameter $D = \mathcal{T} + \lambda_1 + \lambda_2$ is the magnetic thickness of the junction. These parameters are all linked in Josephson junction through the electromagnetic wave velocity $1/\sqrt{\mathcal{C}\mathcal{L}} = \sqrt{(\mathcal{T}/D)/\mu_0\varepsilon_0\varepsilon_r}$ in the oxide barrier.

We study the perturbed sine-Gordon model in the following form,

$$\varphi_{tt} - \varphi_{xx} + \sin \varphi = \eta_{dc} + \eta_{ac} \sin \omega_d t + \Gamma k \sin kx - \alpha \varphi_t + n(x, t) \quad (1)$$

$$\langle n(x, t) \rangle = 0 \quad (2)$$

$$\langle n(x, t)n(x', t') \rangle = 2\alpha\theta\delta(x - x')\delta(t - t') \quad (3)$$

$$\varphi(x, t) = \varphi(x + l, t) + 2\pi, \quad (4)$$

where $\varphi(x, t)$ is the phase difference between the quantum mechanical wave functions of the two superconductors defining the junction. Equations (1)-(4) model an annular Josephson junction of inner radius R and width W when a dc magnetic field is applied in the plane of the junction and the forcing terms include dc and ac currents as well as thermal noise. Assuming uniform Josephson supercurrent pair density j_c over the area of the junction, the critical current density (per unit length) is Wj_c . This is also the characteristic current density against which all current densities are measured in the normalized equations (1)-(4). Tunneling of Cooper pairs of electrons is described by the $\sin \varphi$ term length. Dissipative quasi-particle current density is represented by the term proportional to $\alpha = \mathcal{G}\hbar\omega_p/2eWj_c$

where ω_p is the unperturbed plasma frequency $\omega_p = \sqrt{\frac{2\pi W j_c}{\Phi_0 C}}$ and where $\Phi_0 = \frac{h}{2e} \approx 2.07 \cdot 10^{-15} Wb$ is the flux quantum. The spatial coordinate x is normalized to the Josephson penetration depth $\lambda_J = \sqrt{\frac{\Phi_0}{2\pi \mathcal{L} W j_c}}$ while the temporal coordinate t has been normalized to ω_p^{-1} . An external magnetic field in the plane of the junction (see Fig. 1) is represented by $\Gamma^{10,11}$, which is normalized to the characteristic field $H_0 = j_c \lambda_J$. Given the annular geometry, the effect of the magnetic field is a spatially harmonic potential function with periodicity $l = \frac{2\pi(R+W/2)}{\lambda_J}$ the normalized length of the junction; thus, $k = 2\pi/l$. The junction is driven by a dc current, an ac current, and a thermal noise current from the dissipative quasi-particle term proportional to α , represented by the normalized quantities η_{dc} , η_{ac} and ω_d , as well as n , where n is given by the dissipation fluctuation relationship of Eqs. (2) and (3)¹³. The normalized temperature θ is measured relative to the characteristic temperature $T_0 = E_J/k_B$, where $E_J = \frac{\Phi_0 W j_c}{2\pi}$ is the Josephson energy density. Finally, since we consider only the situation of a single trapped flux quantum, we always impose the boundary condition of Eq. (4).

As outlined in Refs.^{10,11}, the dynamics of an annular Josephson junction with a single trapped fluxon (flux quantum) should behave similarly to a small-area Josephson junction, which in turn is typically modeled by a pendulum equation¹². This can be illustrated by defining the wave momentum P ,

$$P = -\frac{1}{8} \int \varphi_x \varphi_t dx, \quad (5)$$

and using the standard kink-soliton solution,

$$\varphi_s = 4 \tan^{-1} \left[\exp \left(-\frac{x - x_0 - ut}{\sqrt{1 - u^2}} \right) \right], \quad (6)$$

where $u = \dot{x}_0$ and the resulting fluxon momentum is $P = u/\sqrt{1 - u^2}$. We then obtain the following dynamical equation for the fluxon position, x_0 :

$$\frac{dP}{dt} = \frac{\pi}{4} \eta_{dc} + \frac{\pi}{4} \eta_{ac} \sin \omega_d t - \alpha P - \frac{\pi}{4} \Gamma k \operatorname{sech} \left(\frac{1}{2} \pi k \sqrt{1 - u^2} \right) \sin k x_0 + \nu(t). \quad (7)$$

The thermal fluctuation term associated with the fluxon is¹⁴

$$\langle \nu(t) \rangle = 0 \quad (8)$$

$$\langle \nu(t) \nu(t') \rangle = \frac{1}{4} \frac{\alpha \theta}{\sqrt{1 - u^2}} \delta(t - t'). \quad (9)$$

In the following, we restrict the analysis to the non-relativistic limit, $\sqrt{1-u^2} \rightarrow 1$. In this limit, the above equation is equivalent to the usual pendulum model for a small Josephson junction, and for $\theta = \alpha = \eta_{ac} = 0$, we can directly determine the critical current $\eta_c^{(f)}$ and linear plasma oscillation of the fluxon $\omega_p^{(f)}$:

$$\eta_c^{(f)} = \Gamma k \operatorname{sech} \left(\frac{\pi k}{2} \right) \quad (10)$$

$$\omega_p^{(f)} = \sqrt{\frac{\pi}{4} k \sqrt{\left(\eta_c^{(f)}\right)^2 - \eta_{dc}^2}}, \quad (11)$$

where $\eta_c^{(f)}$ is the maximum dc bias current for which zero-voltage states are possible in the system, and $\omega_p^{(f)}$ is the small amplitude oscillation frequency of the fluxon in the washboard potential for $\eta_{dc} \leq \eta_c^{(f)}$. The corresponding equilibrium location of the static fluxon is given by

$$\bar{x}_0 = k^{-1} \sin^{-1} \left(\frac{\eta_{dc}}{\eta_c^{(f)}} \right). \quad (12)$$

These expressions are derived for $\alpha = n = \eta_{ac} = 0$, $l \gg 1$, and small to moderate values of Γ , and arise from a collective coordinate treatment of the fluxon. Thus, the results account neither for spatial fluxon deformation due to the perturbation terms nor for the periodic boundary conditions.

The very close analogy between the behavior of a long annular Josephson junction with a single trapped fluxon in a magnetic field, and a small area Josephson junction has led to several theoretical and experimental studies. One of the latest is the investigation to identify macroscopic quantum tunneling, triggered by the application of microwave radiation, of a flux quantum through the effective washboard potential barrier⁹. Since it was recently demonstrated¹⁵ that the signatures in anomalous switching distributions obtained from small-area Josephson junctions, generated by the application of ac perturbations and attributed to quantum levels, can be reproduced in the classical pendulum model and in experiments conducted at temperatures well above the quantum transition temperature, it is logical to anticipate the same overlap in signatures between the published experimental low temperature results and the classical fluxon behavior.

To investigate the relationship between the classical model and the experimental observations reported in Ref.⁹, we have conducted extensive numerical simulations of the statistics

of thermal fluxon escape from the magnetic-field-induced potential barrier in a manner similar to the experiments. The system is initiated with a trapped fluxon, a given magnetic field Γ , and a dc bias current well below the critical value, $\eta_c^{(f)}$. Thermal noise and an ac bias current at a given frequency are also applied. The dc bias current is continuously increased, typically with a normalized rate of $\dot{\eta}_{dc} \leq 10^{-6}$. The system is defined to have switched from the "static" zero-voltage state by meeting three conditions: 1) the fluxon position, measured as the position of the largest value of $|\varphi_x|$, exceeds $l/2$, 2) the phase $\langle \varphi \rangle_x - \sin^{-1} \eta_{dc}$ exceeds π , and 3) the normalized voltage $\langle \dot{\varphi} \rangle_x$ exceeds $\frac{1}{4}$ of the normalized voltage corresponding to the perturbation estimate of the steady fluxon motion when $\Gamma = 0^{10}$:

$$\langle \dot{\varphi} \rangle_x \Big|_{\Gamma=\eta_{ac}=n=0} = \frac{\pi \eta_{dc}}{\sqrt{(4\alpha)^2 + (\pi \eta_{dc})^2}}. \quad (13)$$

All three switching criteria yield nearly identical switching distributions for $\dot{\eta}_{dc} \lesssim 3.5 \cdot 10^{-5}$. For the very fast sweeps, one of the criteria may be activated immediately due to transient effects from the initial conditions. In such a case, we define switching to have happened when all three criteria are fulfilled. The simulations are carried out with a spatial central difference discretization of $dx = 0.025$ and a Verlet temporal integrator with time step, $dt \approx 0.02$. The normalized damping parameter has been chosen here as $\alpha = 0.001$ for all data shown.

We first show the results of a set of simulations of 75,000 switching events for $l = 10$, $\Gamma = 1$, and $\omega_d = 0.2$. Figure 2 shows the resulting probability density $\rho(\eta_{dc})$ for switching at a given value of η_{dc} for different values of the ac amplitude η_{ac} . The density is normalized such that $\int \rho d\eta_{dc} = 1$. For very small values of η_{ac} , we find a single-peaked localized switching distribution for η_{dc} values just below the predicted critical switching current $\eta_c^{(f)}$. However, for increasing ac amplitude, we observe a nontrivial transition to more complicated statistics of the switching events. For η_{ac} in the interval of $5 \cdot 10^{-4} \lesssim \eta_{ac} \lesssim 10^{-3}$, we observe clear evidence of a double-peaked distribution, closely resembling the experimental observations of Ref.⁹, and for ac amplitudes higher than 10^{-3} , we again find a localized single-peak distribution, but centered at a lower η_{dc} value than for $\eta_{ac} = 0$. The origin of the multi-peaked distributions observed experimentally has been interpreted as evidence for the population of different quantum levels of the fluxon in the magnetic-field-induced potential well, which exists in the static state. Given that the model of this paper is classical, we must interpret our results differently.

In the classical system under investigation here, we do not have intrinsic quantum energy levels of the macroscopic flux quantum. However, as in the experiments, distinct resonances between the fluxon oscillation and the ac field may appear when the ac frequency and the fluxon plasma frequency become harmonics of one another; specifically, when they are equal. The applied frequency $\omega_d = 0.2$ used for the simulations of Figure 2, equals the fluxon resonance frequency $\omega_p^{(f)}$ in the bias current vicinity of the secondary peak in the switching distribution for increasing ac amplitude.

This is verified by Figure 3, in which we have displayed the relationship between the location of the secondary (the ac-induced) peak in bias current, and the predicted fluxon resonance frequency. To demonstrate that the multi-peak switching distribution in the classical limit is not limited to particular parameter ranges, we have chosen to show results for $l = 20$, $\Gamma = 0.25$, and $\dot{\eta}_{dc} = 2.5 \cdot 10^{-7}$. These parameters provide a critical fluxon bias current of $\eta_c^{(f)} \approx 0.0699$. Each distribution shown in Figure 3 is for a particular value of the driving frequency ω_d and the corresponding ac amplitude has been optimized to produce multiple peaks of similar content in switching events. Figure 3 shows the predicted, Eq. (4), relationship between the applied frequency and the location of the ac-induced peak as a solid curve. As can be seen, very reasonable agreement is found. We notice, however, that the peak location is consistently shifted slightly down in frequency (down in current) compared to the predicted linear resonance. This slight discrepancy is consistent for all system parameters we have tried (different lengths and magnetic fields). The reason for the variation is that the resonance leading to any switching event is not purely linear, since the fluxon must experience large oscillations in at least a cubic nonlinearity in order to escape the potential well. Thus, the resonance frequencies are depressed by third-order nonlinearities. This can be quantified from the following simple analysis. Let $x_0 = \bar{x}_0 + A$, where \bar{x}_0 is a constant and A represents oscillatory motion of the fluxon around \bar{x}_0 . The non-relativistic, noiseless limit of Eq. (7) then reads :

$$\ddot{A} + \frac{\pi}{4}\eta_c^{(f)} \sin k\bar{x}_0 \cos kA + \frac{\pi}{4}\eta_c^{(f)} \cos k\bar{x}_0 \sin kA = \frac{\pi}{4}\eta_{dc} + \frac{\pi}{4}\eta_{ac} \sin \omega_d t - \alpha \dot{A} . \quad (14)$$

We assume a single-mode solution in the form

$$A = a \sin(\omega_d t + \psi) , \quad (15)$$

which, when inserted into Eq. (14), yields

$$\sin k\bar{x}_0 = \frac{\eta_{dc}}{\eta_c^{(f)} J_0(ka)} \quad (16)$$

$$\frac{\pi}{4}\eta_{ac} \sin(\omega_d t - \psi) = a \left[\frac{\pi}{2} k \eta_c^{(f)} \frac{J_1(ka)}{ka} \cos k\bar{x}_0 - \omega_d^2 \right] \sin \omega_d t + \alpha a \omega_d \cos \omega_d t. \quad (17)$$

In the low dissipation limit, this results in the amplitude-dependent resonance frequency

$$\omega_{res}^{(f)} = \sqrt{\frac{\pi}{2} k \eta_c^{(f)} \frac{J_1(ka)}{ka} \sqrt{1 - \left(\frac{\eta_{dc}}{\eta_c^{(f)} J_0(ka)} \right)^2}}. \quad (18)$$

Notice that for small amplitude oscillations with $|ka| \ll 1$, Equations (11) and (18) coincide. For larger oscillation amplitudes a , however, we observe a decrease in both critical current and resonance frequency. For multi-peaked switching distribution, as observed in Figure 3, obtained for relatively low temperature θ , the dynamics must be such that the driven oscillations of the fluxon have an amplitude similar to the distance from the energetic minimum position to the corresponding energetic saddle position of the washboard potential; i.e., we can estimate the relevant amplitude of oscillations for multi-peaked distributions to be given by

$$ka \lesssim \pi - 2 \sin^{-1} \left(\frac{\eta_{dc}}{\eta_c^{(f)} J_0(ka)} \right) \quad (19)$$

$$\Rightarrow J_0(ka) \cos \frac{ka}{2} \approx \frac{\eta_{dc}}{\eta_c^{(f)}}. \quad (20)$$

A polynomial expansion of the left-hand side of Eq. (20) for small ka yields the following approximate relationship between the fluxon oscillation amplitude and the bias current:

$$ka \approx \sqrt{\frac{4}{3} \left[1 - \frac{\eta_{dc}}{\eta_c^{(f)}} \right]}. \quad (21)$$

Inserting Eq. (21) into Eq. (18) provides an estimate of the anharmonic resonance frequency relevant for resonant multi-peaked switching distributions. This relationship, $\omega_{res}^{(f)}$ as a function of η_{dc} , is shown in Figure 3 as a dashed curve. We clearly see the depression of the resonance and the very good agreement with the numerical simulations. We notice that fitting the critical bias $\eta_c^{(f)}$ in the linear resonance curve shown in Eq. (11) will lead to very good agreement between simulation results as well, but it is important to emphasize

that while Eqs. (18) and (21) are approximate expressions they do not contain any fitting parameters.

Further investigations of the ac-induced multi-peaked switching distributions and the relationship to the above perturbation analysis are shown in Figure 4 for a system with parameters $l = 10$, $\dot{\eta}_{dc} = 10^{-6}$, and $\Gamma = \frac{1}{4}, \frac{1}{2}, \frac{3}{4}$. We show here only the locations of the ac-induced switching distribution peaks as markers along with the corresponding linear resonance (Eq. (11), solid) and anharmonic resonance (Eqs. (18) and (21), dashed). Again we find very good consistency between the simulated secondary resonant switching peaks and the approximate resonance curves. We see a slight discrepancy developing for increasing magnetic field Γ . This arises due to the strong sensitivity of the perturbation result to the predicted critical current as given by Eq. (10). Figure 5 shows the predicted critical bias as lines together with the corresponding values obtained from numerical simulations of Eq. (1) for $\theta = \eta_{ac} = 0$. The agreement is good for most low to moderate values of Γ , but larger magnetic fields show that the predicted value overestimates the actual critical bias. However, even the very slight difference observed for $l = 10$ and $\Gamma = \frac{3}{4}$ gives rise to the discrepancy observed in Figure 4 for $\Gamma = \frac{3}{4}$, and a fine tuning of $\eta_c^{(f)}$ by less than 1% can make the agreement in Figure 4 be near perfect.

The ac-induced resonant escape described above has been analyzed for situations when an applied ac frequency equals the fluxon oscillation resonance. However, one can equally well expect resonant escape when the applied frequency is a simple rational multiple of the resonance frequency, thereby exciting the fluxon oscillations. This is demonstrated by a few switching distributions shown in Figure 6 for parameters $l = 10$ and $\Gamma = 1$. Here, q indicates the relationship between the driving frequency and the excited resonance $q^{-1}\omega_d = \omega_{res}^{(f)}$, giving rise to the left-most (small bias) escape peak. As can be directly observed, both superharmonic and subharmonic resonances can result in ac-induced switching. Furthermore, we observe (for $q = 2$) that more than one resonance may be excited enough to provide more complex thermal switching distributions in some cases.

Figure 7 summarizes an investigation of the effect of the sweep rate $\dot{\eta}_{dc}$. Key parameters here are $l = 10$, $\Gamma = 1$, $\omega_d = 0.2125$, and $\eta_{ac} = 10^{-3}$. As should be expected, switching distributions of different sweep rates differ such that lower sweep rates enhance early (low η_{dc}) switching, simply because more switching attempts can be made for low bias values. Consequently, in the extreme slow sweep simulations ($\dot{\eta}_{dc} = 10^{-8}$) we observe almost all switching

events near the ($q = 1$) resonance ($\eta_{dc} \approx 0.3875$). In the opposite limit ($\dot{\eta}_{dc} = 10^{-4}$), we observe nearly all switching events around (or beyond) the critical bias ($\eta_{dc} \approx \eta_c^{(f)} \approx 0.41$), and we also observe complex switching distributions for these very fast sweeps. In this case the sweep rate is too large for the fundamental resonance to develop within the time that η_{dc} provides fluxon resonances near the driving frequency, and the system consequently does not have significant opportunity to develop a large amplitude resonant state. Between the two extremes of Figure 7, we have distributions of sweep rates that provide distinctly separated switching peaks. We have, therefore, except for data shown in Figures 7 and 8, chosen sweep rates that on the one hand provide multi-peaked distributions that are not artifacts of excessively fast sweep rates, and on the other hand provide simulation times that will yield statistically meaningful switching distributions with our available computer resources. We notice that the nearly single-peak distribution shown for $\dot{\eta}_{dc} = 10^{-8}$ in Figure 7 should not be interpreted as if multi-peaked distributions vanish for slow sweep rates. In fact, multi-peaked distributions for very slow current sweeps will become observable if the ac amplitude η_{ac} is slightly decreased. Likewise, the very fast sweep will reveal the resonant behavior if the ac amplitude η_{ac} is increased. Thus, we note that complex switching distributions may be easily obtained for many meaningful parameters in ac-driven Josephson systems. To emphasize this essential point, we have produced switching distributions for $\dot{\eta}_{dc} = 10^{-8}$ for different values of η_{ac} . The results, shown in Figure 8, clearly show how lowering the ac amplitude is compensating for the low sweep rate, thereby again illuminating the resonant switching behavior associated with the coupling to the applied ac field.

In conclusion, we have thoroughly investigated the classical thermal sine-Gordon analog to the recently published experimental data from an ac-driven, magnetic-field-embedded annular Josephson junction with a single trapped fluxon. As a result of the applied ac perturbations, we can observe resonant behavior of the trapped fluxon, which in turn gives rise to measurable escape signatures closely resembling experimental observations⁹ made in low temperature conditions. Simple considerations of the (anharmonic) resonances responsible for the anomalous switching distributions show very good and consistent agreement between simulation and analytic perturbation results. Since the external ac field creates resonances whose switching distribution signatures coincide with those of possible intrinsic quantum levels and quantum tunneling, we interpret the results as evidence that the identification of multi-peaked switching distributions cannot be unambiguously related to the identification

of quantum levels and quantum tunneling if the anomalous switching distribution is generated with the application of an external ac field. This conclusion is further strengthened by recent experimental and theoretical work¹⁵ demonstrating that multi-peaked switching distributions in small-area Josephson junctions can be induced by an ac perturbation for temperatures well above the quantum transition temperature similarly to what has been reported in the low temperature regime.

Acknowledgments

This work was supported in part by the Computational Nanoscience Group of Motorola Inc. NGJ acknowledges generous hospitality during several visits to the University of Rome "Tor Vergata". We are grateful to Prof. Alan Laub for carefully reading the manuscript.

-
- ¹ J. M. Martinis, M. H. Devoret, and J. Clarke, Phys. Rev. Lett. **55**, 1543 (1985).
 - ² A. Wallraff, T. Duty, A. Lukashenko, and A. V. Ustinov, Phys. Rev. Lett. **90**, 037003 (2003).
 - ³ T. A. Fulton, and L. N. Dunkelberger, Phys. Rev. B **9**, 4760 (1974).
 - ⁴ M. G. Castellano, G. Torrioli, C. Cosmelli, A. Costantini, F. Chiarello, P. Carelli, G. Rotoli, M. Cirillo, and R. L. Kautz, Phys. Rev. B **54**, 15417 (1996).
 - ⁵ S. Han, J. Laponte, and J. E. Lukens, Phys. Rev. Lett. **63**, 1712 (1989).
 - ⁶ A. Wallraff, Y. Koval, M. Levitchev, M. V. Fistul, and A. V. Ustinov, J. Low Temp. Phys. **118**, 543 (2000).
 - ⁷ M. G. Castellano, A. Intelisano, R. Leoni, N. Milanese, G. Torioli, C. Cosmelli, P. Carelli, and F. Chiarello, Int. J. Mod. Phys. B **14**, 3056 (2000).
 - ⁸ N. Grønbech-Jensen, D. B. Thompson, M. Cirillo, and C. Cosmelli, Phys. Rev. B **67**, 224505 (2003).
 - ⁹ A. Wallraff, A. Lukashenko, J. Lisenfeld, A. Kemp, M. V. Fistul, Y. Koval, and A. V. Ustinov, Nature **425**, 155 (2003).
 - ¹⁰ N. Grønbech-Jensen, P. Lomdahl, and M. R. Samuelsen, Phys. Lett. A **154**, 14 (1991).
 - ¹¹ N. Grønbech-Jensen, Phys. Rev. B **45**, 7315 (1992).
 - ¹² see, e.g., A. Barone and G. Paternò, *Physics and Applications of the Josephson Effect* (Wiley,

New York, 1982)

¹³ see, e.g., G. Parisi, *Statistical Field Theory* (Addison-Wesley, 1988).

¹⁴ M. Salerno, E. Joergensen, and M. R. Samuelsen, *Phys. Rev. B* **30**, 2635 (1984).

¹⁵ N. Grønbech-Jensen, M. G. Castellano, F. Chiarello, M. Cirillo, C. Cosmelli, L. Filippenko, R. Russo, G. Torrioli, *Microwave induced thermal escape in Josephson junctions*, cond-mat/0403245

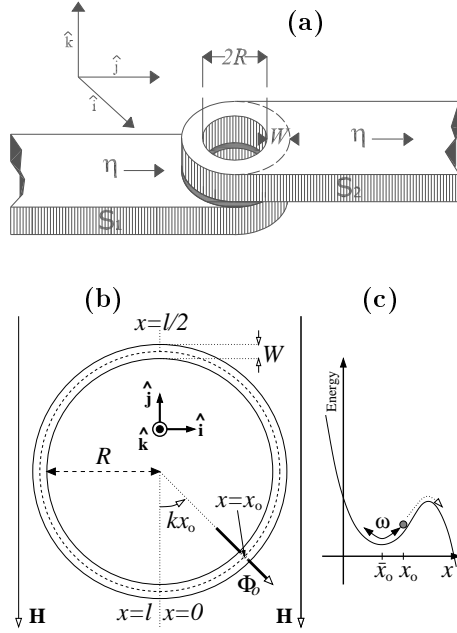


FIG. 1: (a) Sketch of the system under consideration: an annular Josephson junction, defined by the two superconductors \mathbf{S}_1 and \mathbf{S}_2 , with (normalized) bias $\eta = \eta_{dc} + \eta_{ac} \sin \omega dt$; (b) sketch of the trapped flux-quantum orientation and position relative to the external magnetic field \mathbf{H} ; (c) sketch of the magnetic-field-induced washboard potential felt by the flux quantum, which here is illustrated as a particle at position $x = x_0$.

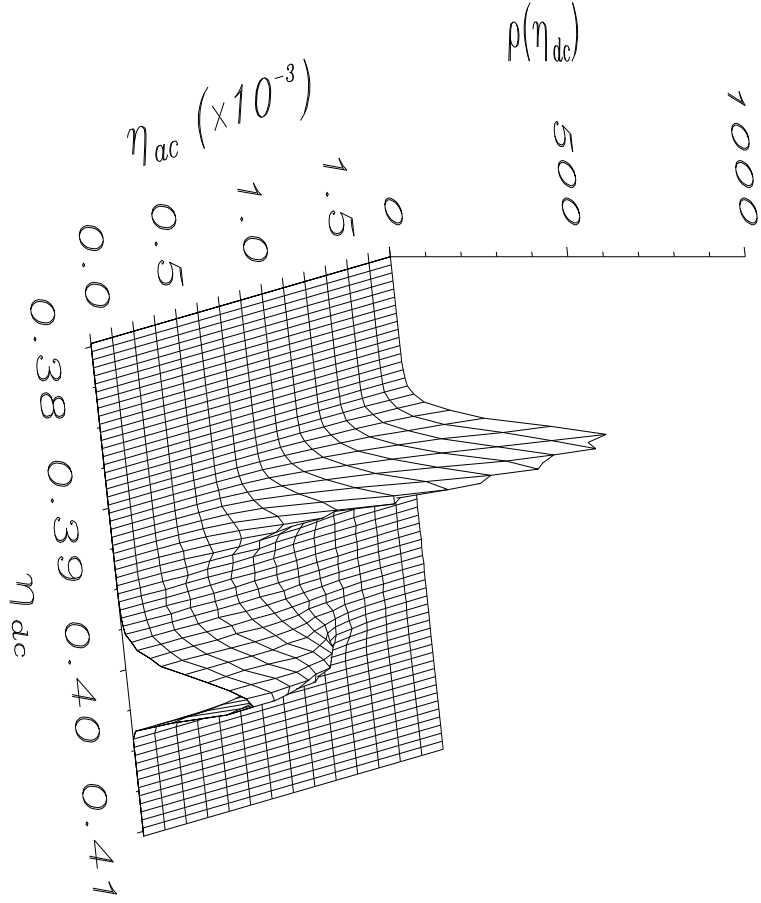


FIG. 2: Simulated switching distributions $\rho(\eta_{dc})$ for $l = 10$, $\Gamma = 1$, $\dot{\eta}_{dc} = 10^{-6}$, $\omega_d = 0.2$, and $\theta = 2.5 \cdot 10^{-3}$. Each distribution represents 5000 switching events.

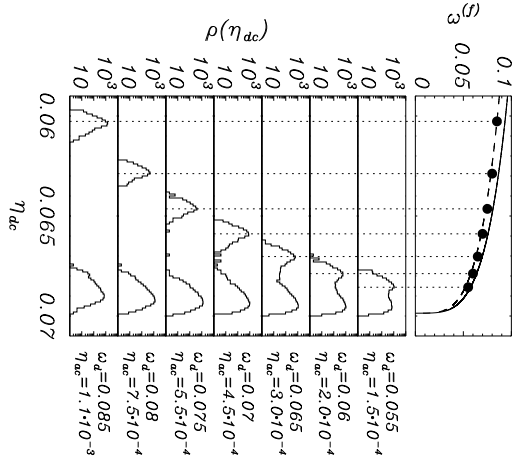


FIG. 3: Simulated switching distributions $\rho(\eta_{dc})$ for $l = 20$, $\Gamma = 0.25$, $\dot{\eta}_{dc} = 2.5 \cdot 10^{-7}$, and $\theta = 10^{-3}$. Each distribution represents 5000 switching events. Top plot shows the linear resonance (solid curve), Eq. (11), and the anharmonic resonance (dashed curve) of Eqs. (18) and (21). Markers (•) show the corresponding frequency-bias relationships as obtained from the ac-induced resonant peaks of the displayed switching distributions.

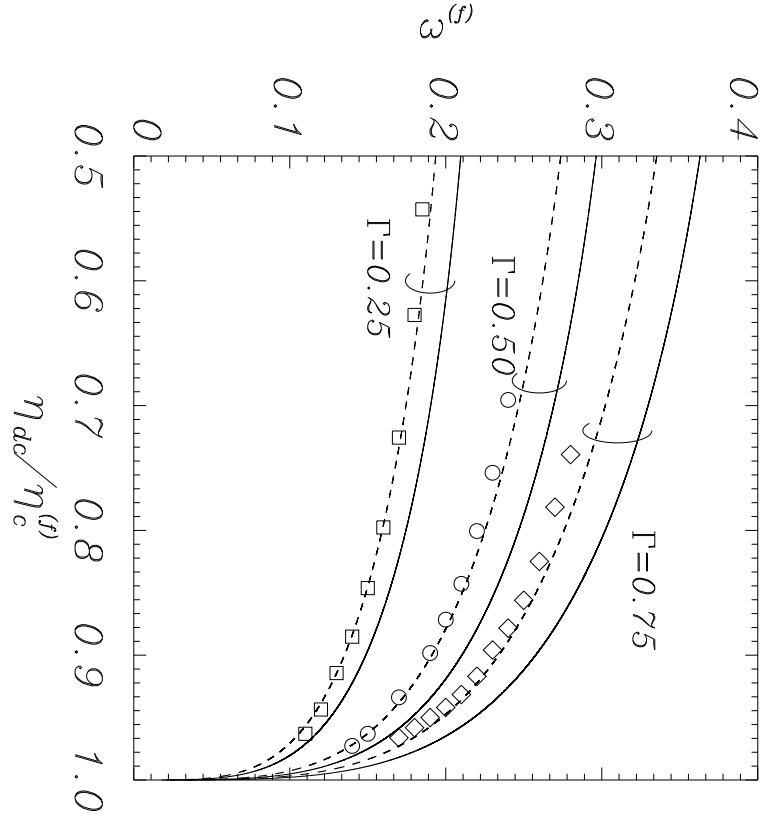


FIG. 4: Simulated relationships between bias and ac-induced oscillation resonance for $l = 10$, $\dot{\eta}_{dc} = 10^{-6}$, and $\theta = 2.5 \cdot 10^{-3}$. Each marker ($\Gamma = 0.25$ \square ; $\Gamma = 0.5$ \circ ; $\Gamma = 0.75$ \diamond) represents a distribution as shown in Figure 3 with 5000 switching events. Solid curves represent the linear resonance, Eq. (11), and the dashed curves represent the anharmonic resonance of Eqs. (18) and (21).

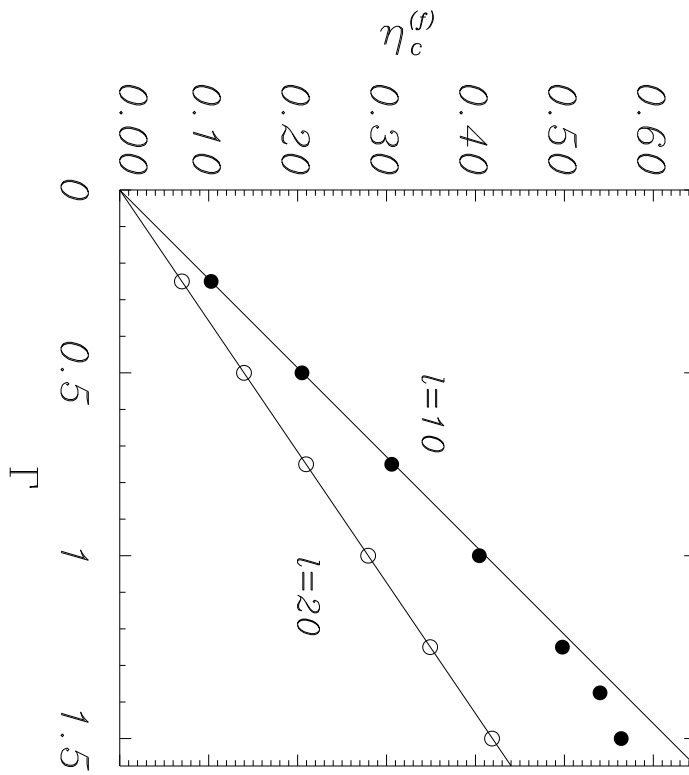


FIG. 5: Comparisons between the predicted critical bias (solid lines) from Eq. (10) and simulated values ($l = 10$ \bullet ; $l = 20$ \circ) for $\theta = \eta_{ac} = 0$.

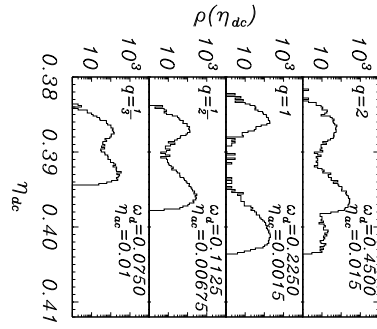


FIG. 6: Simulated ac-induced switching distributions for various harmonics (q) of the same frequency, $\omega_d = q \cdot 0.225$. Parameters are: $l = 10$, $\Gamma = 1$, $\dot{\eta}_{dc} = 10^{-6}$, and $\theta = 2.5 \cdot 10^{-3}$. Each distribution represents 5000 switching events.

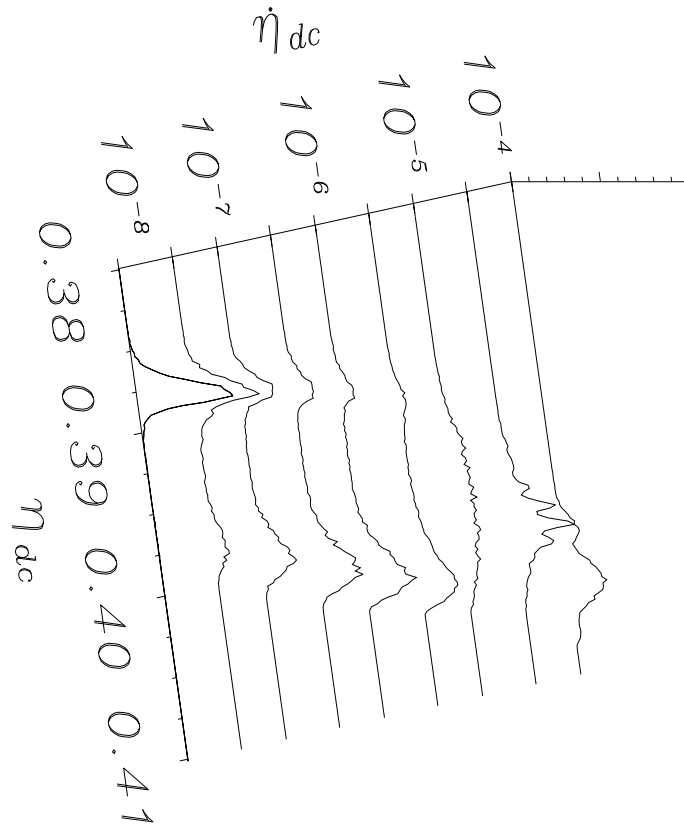


FIG. 7: Simulated switching distributions $\rho(\eta_{dc})$ for $l = 10$, $\Gamma = 1$, $\omega_d = 0.2125$, $\eta_{ac} = 10^{-3}$, and $\theta = 2.5 \cdot 10^{-3}$. Each distribution represents at least 5000 switching events.

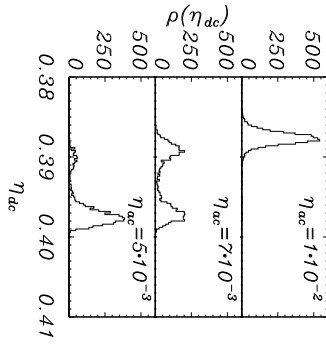


FIG. 8: Simulated switching distributions $\rho(\eta_{dc})$ for $l = 10$, $\Gamma = 1$, $\omega_d = 0.2125$, $\dot{\eta}_{dc} = 10^{-8}$, and $\theta = 2.5 \cdot 10^{-3}$ for three different ac-amplitudes: $\eta_{ac} = 10^{-3}$ (top), $\eta_{ac} = 7 \cdot 10^{-3}$ (middle), $\eta_{ac} = 5 \cdot 10^{-4}$ (bottom). Each distribution represents at least 2000 switching events.